

Edge-guided Multi-domain RGB-to-TIR image Translation for Training Vision Tasks with Challenging Labels

Dong-Guw Lee¹, Myung-Hwan Jeon², Younggun Cho³, Ayoung Kim^{1*}

Abstract—The insufficient number of annotated thermal infrared (TIR) image datasets not only hinders TIR image-based deep learning networks to have comparable performances to that of RGB but it also limits the supervised learning of TIR image-based tasks with challenging labels. As a remedy, we propose a modified multidomain RGB to TIR image translation model focused on edge preservation to employ annotated RGB images with challenging labels. Our proposed method not only preserves key details in the original image but also leverages the optimal TIR style code to portray accurate TIR characteristics in the translated image, when applied on both synthetic and real world RGB images. Using our translation model, we have enabled the supervised learning of deep TIR image-based optical flow estimation and object detection that ameliorated in deep TIR optical flow estimation by reduction in end point error by 56.5% on average and the best object detection mAP of 23.9% respectively. Our code and supplementary materials are available at <https://github.com/rpmsnu/sRGB-TIR>.

I. INTRODUCTION

Recent works on robotics and computer vision have raised interests in the use of thermal infrared (TIR) imaging due to its robustness in environments with harsh weather and poor illumination. Despite this perceptual robustness, TIR cameras induce images with low contrast, poor resolution, and ambiguous object boundaries. In particular, such characteristics instigate performance degradation when applying traditional computer vision methods to TIR images [1]. Deep learning is used as an alternative option to overcome such limitation, yet existing models trained on RGB images hardly adapt well to TIR images, and the number of annotated TIR image datasets are insufficient for training TIR-image-based models with sufficient performance for various tasks.

Different solutions are available to overcome lack of well-annotated labels for TIR. One way is to employ manual annotations by humans, but it is expensive and labor-intensive. Another way is to obtain annotated data from computer simulations, however, obtaining realistic TIR data require sophisticated TIR object priors [2]. Recent method addresses the problem with self-supervised methods [3],

[†]This research was jointly supported by Korea Institute for Advancement of Technology(KIAT) grant funded by the Korea Government(MOTIE) (P0020536, HRD Program for Industrial Innovation) and Institute of Information & communications Technology Planning & Evaluation (IITP) grant funded by the Korea government(MSIT) (No.2022-0-00480, Development of Training and Inference Methods for Goal-Oriented Artificial Intelligence Agents) and (No.2022-0-00448, Deep Total Recall).

¹ D. Lee and A. Kim are with the Dept. of Mechanical Engineering, SNU, Seoul, S. Korea [donkeymouse, ayoungk@snu.ac.kr

² M. Jeon is with the Institute of Advanced Machines and Design, SNU, Seoul, S.Korea myunghwan.jeon@snu.ac.kr

³ Y. Cho is with the Dept. Electrical Engineering of Inha University, Incheon, S. Korea yg.cho@inha.ac.kr

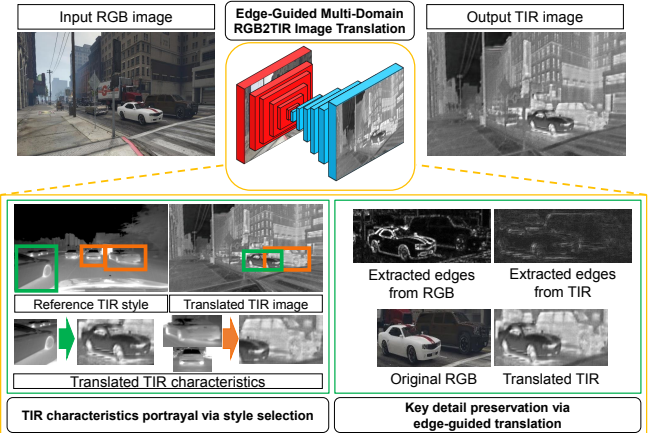


Fig. 1: Our proposed RGB to TIR translation network not only preserves key details in the translated images via edge-guided translation but it also portrays characteristics of thermal images, i.e.g. the undercarriage of the car is heated in the translated image just like the original TIR image.

while careful initialization and pseudo-labeling were required for comparable performances.

Alternative solutions are proposed in [4–6] who utilized Generative Adversarial Network (GAN)-based image translation methods; these methods obtain annotated TIR image data from translating RGB images into TIR images and leveraging annotations from RGB data. In fact, Hou et al. [2] argues that for TIR image-based semantic segmentation, leveraging GAN-based translation is much simpler but more accurate way to account for the lack of data than obtaining synthetic TIR data from simulations.

GAN-based RGB to TIR translation methods have actively been studied in the past [7–11], yet existing *bi-domain*-based image translation methods leverage deterministic bijective mapping function to directly map each pixel in the RGB domain to that of TIR. As a consequence, such methods can incur artifacts in the translated TIR images when input images differ greatly from the training images and are not suitable translation method for tasks that require image style consistency between two input frames. Contrastive learning-based methods [12, 13] tried to overcome these shortcomings, yet matching semantic relations between two domains with large semantic discrepancies can be difficult without additional constraints or loss functions. More importantly, translated image styles cannot be controlled with such bi-domain-based methods.

On the other hand, we propose an edge-guided *multi-domain* image translation network to translate RGB to TIR images. Multi-domain translation network refers to methods that use disentangled content and style latent vectors for image translation [14]. Consequently, artifacts in the translated

images could be minimized by selecting the suitable TIR style for target RGB image, and image consistency between two consecutive image frames can be maintained. In addition, edge-guided loss is used to preserve the key dynamic details in the translated TIR image. The two highlights of our proposed method are illustrated in Fig. 1.

Most importantly, no existing study has hardly leveraged RGB to TIR translation to train to tasks with extreme level of difficulty in manual labeling. Using our translation network, we not only enabled supervised learning on tasks with challenging labels such as deep optical flow estimation in TIR, but inspired by [15], we also validated the effectiveness of our proposed method in object detection without the need for any manual annotations.

Key contributions of our research as follows:

- 1) We propose an edge-guided and style-controlled multi-domain RGB to TIR translation network. Unlike previous methods, our proposed method leverages the most suitable style vector to generate realistic TIR images with minimum artifacts and also preserve key details in the image regardless of any TIR image styles. Objects in the translated TIR images displayed valid edge consistency to both synthetic and real RGB images.
- 2) We complete a supervised deep TIR optical flow estimation, which is a task with an extreme level of difficulty in manual labeling, at a much lesser effort through the dataset generation with our proposed method. By attaining reliable geometric consistency of the objects between consecutive sequential frames in the translated TIR images, we demonstrated an amelioration in learning-based TIR optical flow estimation.
- 3) We further validate that our translation model can be extended to semantic tasks such as object detection and lessen the human user’s effort in annotations. Our RGB to TIR translation pipeline will be open-sourced for future academic research related to robotics and computer vision.

II. RELATED WORKS

A. Unpaired RGB to TIR image translation

Several past studies have addressed image translation from both RGB to TIR [5–11, 16] and TIR to RGB [4, 17–19], yet, their objectives are completely different. As illustrated in Fig. 2, in the former, the translation network needs to cope with several variations that could exist in the input RGB image, but in the generated output, only monochromatic TIR images are considered. Hence, the translation can be formulated as a multiple input, single output problem. In the latter, however, diverse chromatic translation of pseudo-RGB images is hardly required, thereby formulating single input, single output problem. Considering such definition, we argue that multi-domain translation methods should be leveraged for RGB to TIR image translations.

Despite the need for multi-domain-based translation, recent RGB to TIR translation were based on bi-domain based translation. As a result, they generalized poorly on images

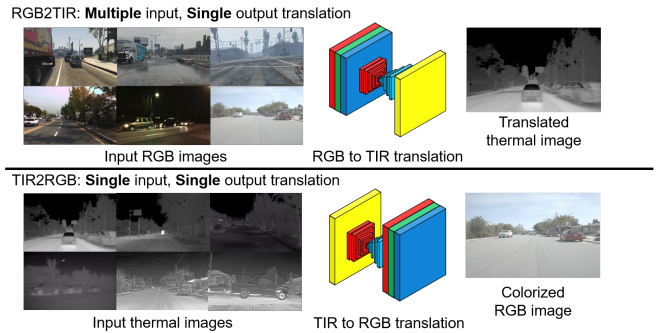


Fig. 2: Main objectives for RGB to TIR and TIR to RGB image translation. The former can be defined as multi-input single-output translation problem, and the latter can be viewed as a single input single output translation problem due to the lesser chrominance variation in TIR images.

that are outside of the training data, and hardly any key details were preserved in the translated image, especially for those methods based on paired image translation model [6, 9, 10, 16]. Especially, these methods were vulnerable to the translation of images with adverse illumination and weather conditions.

On the contrary, our edge-guided multi-domain translation method is more robust to translating unseen RGB images and preserves the key details in the translated image.

B. Deep TIR optical flow estimation

Recent studies on thermal-inertial odometry [3, 20, 21] have actively incorporated deep learning-based TIR optical flow estimation models due to their superior performance over the classical methods [22]. However, due to the extreme difficulty in obtaining ground truths flow, even for RGB images [23], deep optical flow estimation model, preinitialized on synthetic RGB images, were used to compute optical flow from TIR images [20, 21]. Consequently, erroneous TIR optical flow could be expected due to the domain discrepancies between TIR and synthetic RGB images.

On the contrary, we enabled the training of deep TIR optical flow estimation model in a supervised manner. Our proposed method not only surpassed the optical flow estimation that adhered to that of Saputra et al. [20], but also no additional separate RGB teacher networks are needed. In addition, compared with self-supervised methods, our method does not need any explicit and carefully designed pseudo flow generation [3].

III. PROPOSED METHOD

A. Network overview

1) *Key Notations*: Listed below are the notation used in the paper.

- $G_{TIR}, G_{RGB}, D_{TIR}$: TIR decoder, RGB decoder, TIR discriminator. The decoder acts as the generator.
- x_{RGB}, x_{TIR} : Input RGB and TIR images.
- E_{RGB}^c, E_{RGB}^s and E_{TIR}^c, E_{TIR}^s : Content and style encoder for RGB and TIR images.
- c_{RGB}, s_{RGB} and c_{TIR}, s_{TIR} : Latent content and style vector for RGB and TIR images.

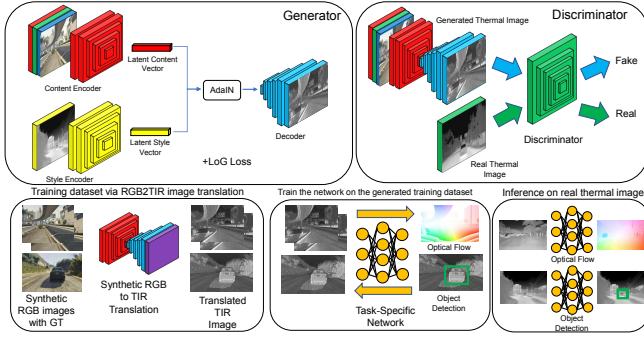


Fig. 3: RGB to TIR translation network and overall training pipeline. The encoders are divided into the content encoder (red) and a style encoder (yellow). Each encoder disentangles an image into each latent content and style vector. The decoder (blue) integrates the content and the style vector via adaptive instance normalization (AdaIN) [24] and generates the translated image. The role of the discriminator (green) is to classify the input image as either a real or a fake image. Using the translation model, synthetic RGB images with corresponding ground truths labels are translated into TIR images, formulating TIR image dataset with ground truths labels. Using the translated dataset, it can be leveraged to train any task-specific network in a supervised manner. Best viewed in color.

2) *Network Architecture*: We adopted GAN-based multi-domain unpaired image to image translation architecture [25] as our baseline architecture. As illustrated in Fig. 3, the generator is composed of two encoders and a single decoder. Having contents and style vectors encoded from each encoder, the content encoder encapsulates the geometric attributes of an image such as edges and outlines of an image; the style encoder encapsulates the color and pixel intensity characteristics of TIR images.

3) *Loss functions*: We employed adversarial loss [26] for training GAN and style-augmented cyclic loss, L_{cyc} [25], to enforce additional cyclic consistency. We also used three types of reconstruction losses to enforce edge-guided and multi-domain translation. Although the translation is bidirectional, only the losses that are appropriate to RGB to TIR translation will be expressed.

Image reconstruction Loss: Concerns the ability of the translation network to reconstruct the original RGB image.

$$\mathcal{L}_{recon}^{x_{RGB}} = \mathbb{E}[||G_{RGB}(E_{RGB}^c(x_{RGB}), E_{RGB}^s(x_{RGB})) - x_{RGB}||_1] \quad (1)$$

Content and Style Reconstruction Loss: Related to the ability to extract valid latent content and style vectors from given images. As content vector from a RGB image is needed for generating the translated TIR image, the content reconstruction loss computes the difference between the content vector of the original RGB image and that of the translated TIR image.

$$\mathcal{L}_{recon}^{c_{RGB}} = \mathbb{E}[||E_{TIR}^c(G_{TIR}(c_{RGB}, s_{TIR})) - c_{RGB}||_1] \quad (2)$$

Similarly, the style reconstruction loss computes the difference between the style vector of the original TIR image and that of the translated TIR image.

$$\mathcal{L}_{recon}^{s_{TIR}} = \mathbb{E}[||E_{TIR}^s(G_{TIR}(c_{RGB}, s_{TIR})) - s_{TIR}||_1] \quad (3)$$

Laplace of Gaussian (LoG) Loss: Since unpaired RGB to TIR image translation methods [25, 27, 28] were severely under-constrained, we imposed additional constraints that can enforce the texture and edge consistency in the translated image. To achieve this, we utilized LoG loss [29]

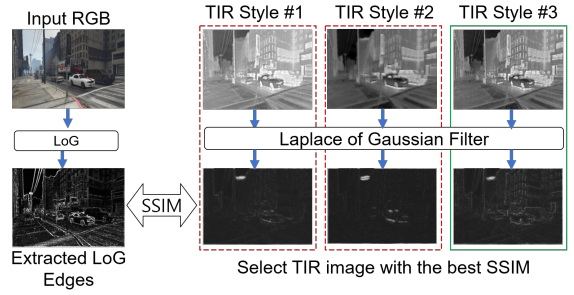


Fig. 4: Our proposed optimal style selection module. Edges of input RGB and several TIR images are extracted from LoG filters, and SSIM between the RGB edge and each TIR edge are computed. TIR image with the best SSIM score is selected as the optimal style of the translation model.

between the original and the reconstructed image computes the distance between the extracted Laplacian features of the original and the reconstructed image. It penalizes the network for generating images with second order gradient-based edge dissimilarity. The Laplacian features can be extracted by first applying a 3×3 Laplacian filter to each image channel ($x_{TIR}^1 \dots x_{TIR}^3$), follow by global-average pooling the extracted features from each channel, like shown in (4). Unlike other edge-guided losses, LoG loss does not require any auxiliary edge extraction network for multi-task learning [30, 31].

$$\mathcal{L}_{Lap} = \mathbb{E}[||L(x_{TIR}) - L(x_{TIR, recon})||_1] \quad (4)$$

$$L(x_{TIR}) = \frac{1}{3}(L(x_{TIR}^1) + L(x_{TIR}^2) + L(x_{TIR}^3))$$

4) *Overall training objective*: The overall training objectives of the network are shown in (5). All encoders, decoders, and discriminators are jointly trained and then optimized. The overall loss function is computed by a weighted sum of several different losses.

$$\mathcal{L}_G = \mathcal{L}_{GAN} + \lambda_{x_{recon}} \mathcal{L}_{recon}^{x_{TIR}} + \lambda_{c_{RGB}} \mathcal{L}_{recon}^{c_{RGB}} + \lambda_{s_{TIR}} \mathcal{L}_{recon}^{s_{TIR}} + \lambda_{Lap} \mathcal{L}_{Lap} + \lambda_{cyc} \mathcal{L}_{cyc} \quad (5)$$

For training the proposed image translation model, the loss weighting coefficients, $\lambda_{x_{recon}}, \lambda_{c_{RGB}}, \lambda_{s_{TIR}}, \lambda_{Lap}$, and λ_{cyc} were set to 20, 10, 10, 20, and 5 respectively.

B. Translation style selection

A clear advantage of multidomain image to image translation (e.g. MUNIT) over bi-domain image translation (e.g. CycleGAN) is that the style of the translated image can be controlled with a given style code. By utilizing multi-domain translation, we can select TIR style codes which has the least domain discrepancies to that of the input RGB image. By selecting the appropriate style from multiple sample style codes that were generated from various TIR images, artifacts or erroneous patches can be minimized and characteristics of TIR images can be accurately portrayed.

As described in Fig. 4, the style selection procedure is executed in the following way. First, using our proposed multi-domain RGB to TIR translation model, we sample multiple translated TIR images with different style codes. Second, we leveraged a 3×3 LoG filter to extract the edges from both the input synthetic RGB image and the translated TIR images with different style codes.

Inspired by the works of Luo et al. [19], we computed structural similarity index measurement (SSIM) between the extracted LoG edges of the input RGB image and each extracted LoG edge corresponding to the translated TIR image with different style codes. We conjecture that higher SSIM would refer to lesser number of artifacts created in the image but at the same time accurately portrayed the characteristics of TIR image in the translated image well.

For optical flow estimation, not only accurate TIR characteristics need to be portrayed, especially for dynamic objects that correspond to ground truths flow, but the style of the translated images between the input image pair also needs to be consistent. We can achieve the input translated image pair consistency by translating the image pair with the same style codes.

IV. EXPERIMENTAL SETUP

A. Synthetic RGB to TIR image translation

1) *Training dataset*: We leveraged several public benchmark datasets to train our proposed network in an unpaired manner. For RGB images, we utilized VIPER [32]. For TIR images, we combined FLIR-ADAS [33] and STheReO [34]. Overall, 13,554 RGB and 21,424 TIR images were used. Details on the network architecture and parameters are available on our project page.

2) *Training details*: We trained our proposed method against two bi-domain-based methods (CycleGAN [27] and UNIT [28]) and a single multi-domain-based method, MUNIT [25]. All models were trained using only synthetic RGB images and real TIR images.

We used input image with resolution of 640×400 for both RGB and TIR images. For the network hyperparameters, we used Adam optimizer with a learning rate of 0.0001, weight decay of 0.5, 0.5 and 0.99 as β_1 and β_2 respectively. The network was trained for batch size of 1 for 60,000 iterations.

3) *Evaluation criteria*: We evaluated our translation model using average precision canny edge (APCE) [19], which computes the average precision of extracted canny edges between RGB and the translated TIR images at different thresholds.

B. Deep supervised TIR optical flow estimation

1) *TIR image-based optical flow dataset*: To train the deep TIR image-based optical flow estimation model, we first employed our proposed synthetic RGB to TIR image translation model to the VIPER dataset. Overall, this yielded 13,356 and 4,954 optical flow image pairs and their corresponding flow ground truths labels for each training and validation data.

2) *Training details*: We employed recent state of the art deep optical flow estimation architectures, namely RAFT [35], GMA-RAFT[36], and GMFlow[37]. For training deep TIR optical flow estimation models, we followed the practices of [3] where we first train the model on synthetic RGB images for several epochs. Afterwards, we finetuned the trained model on our TIR optical flow dataset. We employed random horizontal flip for data augmentations. As for the training hyperparameters, all three optical flow models were

trained for 100,000 iterations at a batch size of 12 and were optimized using Adam optimizer with β_1 and β_2 as 0.5 and 0.99. Each RAFT, GMA-RAFT, and GMFlow leveraged learning rates of 0.0004, 0.00002, and 0.00002 with weight decay of $1e-4$, $5e-5$, and $5e-5$ respectively.

3) *Evaluation Criteria*: To quantitatively evaluate the performance of our TIR optical flow estimation model, we translated validation optical flow dataset of VIPER into TIR images. We evaluated our TIR optical flow estimation model and preinitialized deep optical flow model on the TIR VIPER validation set using average end-point error (EPE). In addition, we use flow visualizations to qualitative evaluate the optical flow models on real TIR images from several benchmarking TIR-image datasets.

V. RESULTS AND DISCUSSION

A. Edge-guided multi-domain RGB to TIR translation

We evaluated our proposed methods and the baselines on RGB images from synthetic RGB image datasets (VIPER [32], Synthia [38], Sintel [39], and Virtual Kitti [23]) and real world RGB image datasets (STheReO, KAIST [40], and FLIR-ADAS).

The translation results for the generated TIR images from synthetic and real RGB images are illustrated in Fig. 5 and Fig. 6. From a qualitative point of view, our proposed method outperformed other baselines in both synthetic RGB and real RGB image translations. The proposed method was able to maintain edge consistency as well as TIR image characteristics, as indicated by the green boxes. In particular, unlike the poor translation results from other baseline methods, our method successfully maintained key details in Sintel-2, Virtual KITTI, and FLIR Day 1 images, and even small details presented in the FLIR Day 2 image were portrayed in the TIR image generated using our proposed method. Similarly, the baseline methods either produced additional image artifacts or were unable to retain all the details presented in the original image, as indicated by the red boxes. However, our proposed method was able to translate all key visible details presented in the original RGB images.

More importantly, one of the main bottlenecks of RGB to TIR translation persisted in translating RGB image with poor illumination to TIR images. In the baseline methods, poor TIR image translation results were demonstrated for night time images (Fig. 6). However, TIR image using our method has portrayed valid key details such as cars, showing better robustness to translation of night time images than other baseline methods.

The qualitative evaluation of our proposed translation method can be supported by the quantitative APCE evaluation. Table. I represents the average APCE and per image APCE evaluation for all models in both synthetic and real RGB image translation setting. According to the APCE evaluation, our proposed model outperforms all other baselines in terms of average APCE in both synthetic RGB and real RGB image translations; the same can be applied for per-image APCE except for image translation on Virtual KITTI. Therefore, both qualitatively and quantitatively, our proposed

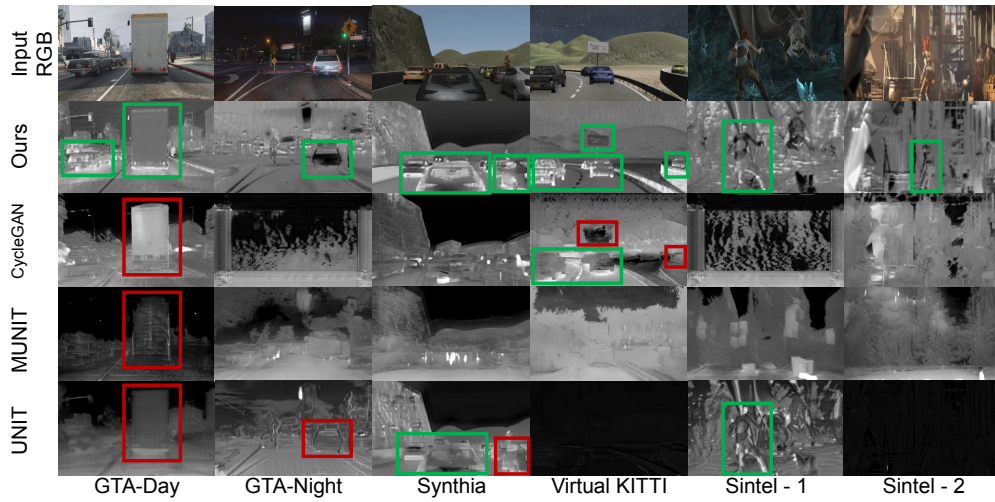


Fig. 5: Comparison of the baseline and the proposed method on synthetic RGB to TIR image translation. Our proposed method has translated key details in the original image (green boxes) whereas the baseline methods fail to generate objects with sharp edges and realistic TIR characteristics (red boxes). In addition, for several instances, the translation either completely fails or key objects within the image disappeared. Our translation method also generalizes well to unseen synthetic RGB datasets. Best viewed in color.

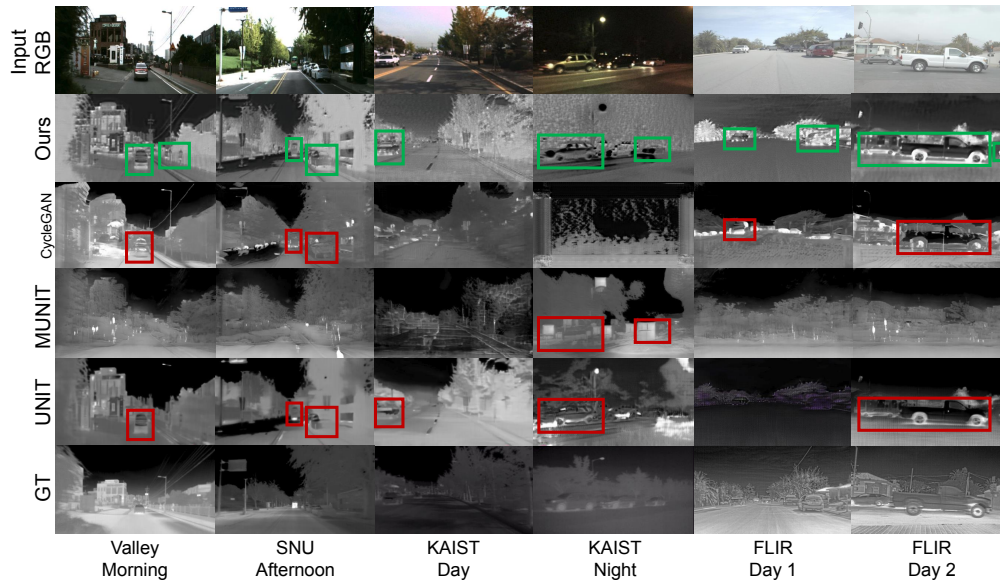


Fig. 6: Comparison of the baseline and the proposed method on real RGB to TIR image translation. Even when trained on synthetic RGB images, our method generalizes well to real world RGB images regardless of the place and illumination condition, and characteristics of TIR images are most accurately portrayed (green boxes). Same as before, artifacts and incorrectly translated objects are portrayed (red boxes); additionally, for some translation instances, key objects (green boxes) disappeared in the translated image. Best viewed in color. For better view of the images in the original size, please check out our project page.

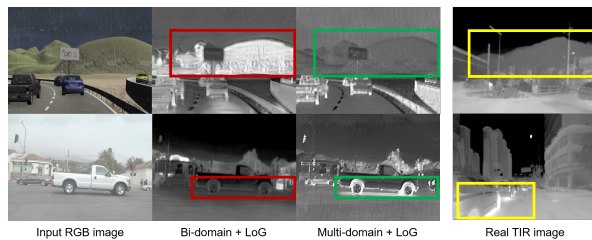


Fig. 7: Comparison of bi-domain model with LoG vs multi-domain with LoG. Realistic characteristics of TIR images (yellow boxes) are well portrayed in the multi-domain methods (green boxes) but not in bi-domain-based methods (red boxes).

translation method outperformed other existing method for translating from RGB to TIR images.

We performed further ablation study to examine the valid use of multi-domain model over bi-domain model in RGB to TIR image translation. For evaluation, we compared our proposed method with a bi-domain model with LoG loss, as presented in Fig. 7.

TABLE I: APCE comparison for various methods on both real and synthetic images

Models	Proposed	CycleGAN	MUNIT	UNIT
Synthetic Images				
GTA-Day	0.0793	0.0495	0.0175	0.0322
GTA-Night	0.1264	0.0351	0.0262	0.0304
Synthia	0.0967	0.0753	0.0289	0.0404
Virtual Kitti	0.1221	0.1516	0.0165	0.0138
Sintel-1	0.1301	0.0606	0.0226	0.0067
Sintel-2	0.1246	0.0398	0.0118	0.0584
Average	0.11	0.07	0.02	0.03
Real Images				
Valley-Morning	0.0936	0.045	0.0232	0.0207
SNU Afternoon	0.1502	0.0354	0.0248	0.0514
KAIST Day	0.1683	0.0658	0.032	0.0389
KAIST Night	0.1432	0.0456	0.0399	0.046
FLIR Day-1	0.0544	0.0395	0.0204	0.0281
FLIR Day-2	0.0943	0.0486	0.0261	0.0451
Average	0.12	0.05	0.03	0.04

By using edge-guided training on the bi-domain model, valid key details were also depicted in the translated TIR image. However, realistic characteristics of thermal images were hardly represented in the translated image. For example, in the bottom image, the TIR image translated using the

TABLE II: End point error evaluation on the our proposed and baseline methods

Model	EPE (RGB)	Training EPE (Thermal)	EPE (Thermal)
RAFT	43.762	3.069	16.18
GMFlow	44.106	8.536	24.568
GMA-RAFT	41.740	2.917	15.733

bi-domain method did not portray any TIR residual heat marks under the car; in contrast, using our proposed method based on multi-domain translation, characteristics of TIR images were depicted in the translated image, indicated by the red boxes. Therefore, even with LoG loss being used to enforce edge in the image, bi-domain-based translation method hardly portrayed the correct characteristics of real TIR images in the translated images.

B. Deep TIR optical flow estimation

The results to the quantitative and the qualitative evaluations are listed in Table. II and Fig. 8. From a qualitative evaluation on real TIR images, our TIR optical flow estimation models has shown better flow estimation performance than the baseline flow estimation model. Indicated by the green boxes, our TIR optical flow model not only yielded sharper and clearer flow estimation on dynamic objects, but it also estimated flow from even smaller objects, which were not present in the preinitialized methods.

We observed ameliorated optical flow estimation performances in all three models that were finetuned on our TIR-image dataset, outperforming the baseline preinitialized models. Out of all three models, GMA-RAFT displayed the lowest EPE, followed by RAFT and GMFlow. Despite the superior performance of GMFlow over RAFT in RGB image-based optical flow estimation, inferior performance was shown in TIR images due to the insufficient number of TIR image-based data to maximize the performance on transformer-based model.

Since the characteristics of TIR image greatly differs from that of RGB, flow estimation via conventionally used methods [20] has resulted in high EPE, yielding inaccurate flow estimation. On the contrary, estimating optical flow using our translated TIR image dataset has yielded a valid performance improvement in real TIR images. Particularly, the TIR optical flow model was able to estimate flow from objects with ambiguous object boundary in the TIR image. From this, we can deduce that our proposed translation method ameliorated TIR optical flow estimation performance on real TIR images when the model was only trained with generated TIR data using our proposed method with RGB optical flow annotations. More importantly, this also demonstrated that our proposed translation model accurately portrayed TIR characteristics in the generated TIR images.

TABLE III: Object detection performance evaluation on FLIR Validation set

Methods	mAP	mAP_50	mAP_75	mAP_S	mAP_M	mAP_L
Proposed	0.239	0.408	0.237	0.061	0.441	0.692
CycleGAN	0.007	0.01	0.01	0	0.005	0.009
MUNIT	0.069	0.137	0.06	0.007	0.117	0.413
UNIT	0.225	0.384	0.222	0.062	0.414	0.671

C. Extension to object detection

To further reveal the performance over semantic tasks, we examined the potential extension of our proposed method to

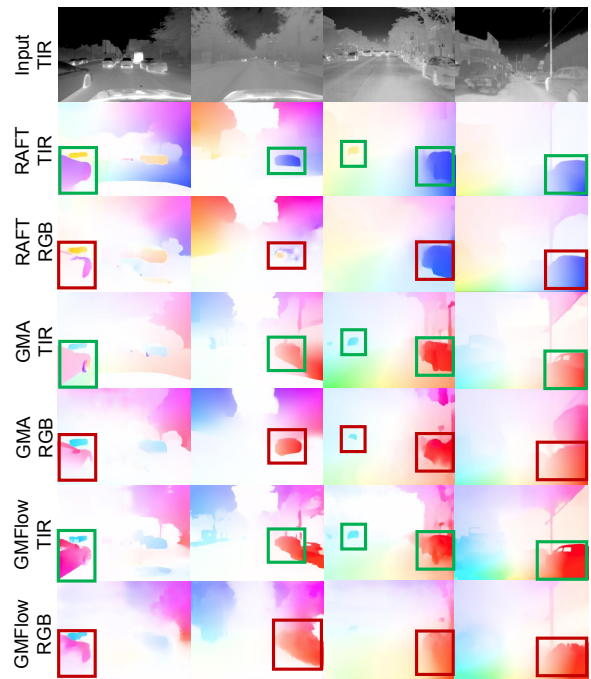


Fig. 8: Flow visualization comparison of various optical flow methods on real TIR images. TIR optical flow estimated by our trained models yielded sharper and more completed flow estimation, and they also yielded flow estimation from smaller objects (green boxes). In contrast, estimated flow from RGB-preinitialized methods resulted in occluded flow with ambiguous boundaries (red boxes).

object detection. For evaluation, we leveraged our proposed method and the baseline networks to generate TIR-image based object detection datasets from a synthetic RGB object detection dataset [41], yielding four individual synthetic TIR datasets. We then trained each dataset individually on VFNet [42]. We validated the trained networks on FLIR-ADAS [33]. The detection performance of the trained models are displayed in Table. III.

According to the detection performance, our method achieved the highest mean average precision (mAP) of 0.239 compared to other methods. Although UNIT has outperformed our proposed method in small object detection by 0.001, our proposed method has outperformed other baseline networks in other evaluation criteria. From these results, we confirm that our proposed method can not only be used for training tasks with challenging labels, but it also can reduce effort for data annotation on other tasks like object detection.

VI. CONCLUSION

Recent learning-based models in robotics and computer vision are becoming more data hungry. Especially, for those tasks with challenging labels such as optical flow, there are limitations to the number of annotated TIR image datasets. This limitation can be addressed by using our edge-guided multidomain RGB to TIR image translation network to generate annotated TIR image dataset from synthetic RGB images. We confirmed the valid use of our proposed method through training deep TIR optical flow and object detection by demonstrating performance improvements compared to other baselines. For further works, we plan to extend our approach to different tasks with challenging labels such as TIR semantic segmentation and 3D object detection.

REFERENCES

- [1] Manash Pratim Das, Larry Matthies, and Shreyansh Daftry. Online photometric calibration of automatic gain thermal infrared cameras. *IEEE Robotics and Automation Letters*, 6(2):2453–2460, 2021.
- [2] Yu Hou, Rebekka Volk, and Lucio Soibelman. A novel building temperature simulation approach driven by expanding semantic segmentation training datasets with synthetic aerial thermal images. *Energies*, 14(2):353, 2021.
- [3] Jiajun Jiang, Xingxin Chen, Weichen Dai, Zelin Gao, and Yu Zhang. Thermal-inertial slam for the environments with challenging illumination. *IEEE Robotics and Automation Letters*, 2022.
- [4] Chaitanya Devaguptapu, Ninad Akolekar, Manuj M Sharma, and Vineeth N Balasubramanian. Borrow from anywhere: Pseudo multi-modal object detection in thermal imagery. In *Proceedings of the IEEE/CVF Conference on Computer Vision and Pattern Recognition (CVPR) Workshops*, June 2019.
- [5] Lichao Zhang, Abel Gonzalez-Garcia, Joost Van De Weijer, Martin Danelljan, and Fahad Shahbaz Khan. Synthetic data generation for end-to-end thermal infrared tracking. *IEEE Transactions on Image Processing*, 28(4):1837–1850, 2018.
- [6] Chenglong Li, Wei Xia, Yan Yan, Bin Luo, and Jin Tang. Segmenting objects in day and night: Edge-conditioned cnn for thermal image semantic segmentation. *IEEE Transactions on Neural Networks and Learning Systems*, 32(7):3069–3082, 2020.
- [7] Yi Luo, Dechang Pi, Yue Pan, Lingqiang Xie, Wen Yu, and Yufei Liu. Clawgan: Claw connection-based generative adversarial networks for facial image translation in thermal to rgb visible light. *Expert Systems with Applications*, 191:116269, 2022.
- [8] Adam Nyberg, Abdelrahman Eldesokey, David Bergstrom, and David Gustafsson. Unpaired thermal to visible spectrum transfer using adversarial training. In *Proceedings of the European Conference on Computer Vision (ECCV) Workshops*, pages 0–0, 2018.
- [9] Mehmet Akif Özkanoglu and Sedat Ozer. Infragan: A gan architecture to transfer visible images to infrared domain. *Pattern Recognition Letters*, 155:69–76, 2022.
- [10] Vladimir V. Kniaz, Vladimir A. Knyaz, Jiri Hladuvka, Walter G. Kropatsch, and Vladimir Mizginov. Thermalgan: Multimodal color-to-thermal image translation for person re-identification in multispectral dataset. In *Proceedings of the European Conference on Computer Vision (ECCV) Workshops*, September 2018.
- [11] Ran Zhang, Junchi Bin, Zheng Liu, and Erik Blasch. Wggan: A wavelet-guided generative adversarial network for thermal image translation. In *Generative Adversarial Networks for Image-to-Image Translation*, pages 313–327. Elsevier, 2021.
- [12] Taesung Park, Alexei A. Efros, Richard Zhang, and Jun-Yan Zhu. Contrastive learning for unpaired image-to-image translation. In *European Conference on Computer Vision*, 2020.
- [13] Junlin Han, Mehrdad Shoeiby, Lars Petersson, and Mohammad Ali Armin. Dual contrastive learning for unsupervised image-to-image translation. In *Proceedings of the IEEE/CVF conference on computer vision and pattern recognition*, pages 746–755, 2021.
- [14] Hsin-Ying Lee, Hung-Yu Tseng, Qi Mao, Jia-Bin Huang, Yu-Ding Lu, Maneesh Singh, and Ming-Hsuan Yang. Dri++: Diverse image-to-image translation via disentangled representations. *International Journal of Computer Vision*, 128:2402–2417, 2020.
- [15] Simon Chadwick and Paul Newman. Radar as a teacher: Weakly supervised vehicle detection using radar labels. In *2020 IEEE International Conference on Robotics and Automation (ICRA)*, pages 222–228. IEEE, 2020.
- [16] My Kieu, Lorenzo Berlincioni, Leonardo Galteri, Marco Bertini, Andrew D Bagdanov, and Alberto Del Bimbo. Robust pedestrian detection in thermal imagery using synthesized images. In *2020 25th International Conference on Pattern Recognition (ICPR)*, pages 8804–8811. IEEE, 2021.
- [17] Xiaodong Kuang, Jianfei Zhu, Xiubao Sui, Yuan Liu, Chengwei Liu, Qian Chen, and Guohua Gu. Thermal infrared colorization via conditional generative adversarial network. *Infrared Physics & Technology*, 107:103338, 2020.
- [18] Dan Tao, Junsheng Shi, and Feiyan Cheng. Intelligent colorization for thermal infrared image based on cnn. In *2020 IEEE International Conference on Information Technology, Big Data and Artificial Intelligence (ICIBA)*, volume 1, pages 1184–1190. IEEE, 2020.
- [19] Fuya Luo, Yunhan Li, Guang Zeng, Peng Peng, Gang Wang, and Yongjie Li. Thermal infrared image colorization for nighttime driving scenes with top-down guided attention. *IEEE Transactions on Intelligent Transportation Systems*, 2022.
- [20] Muhamad Risqi U Saputra, Pedro PB de Gusmao, Chris Xiaoxuan Lu, Yasin Almalioglu, Stefano Rosa, Changhao Chen, Johan Wahlström, Wei Wang, Andrew Markham, and Niki Trigoni. Deeptio: A deep thermal-inertial odometry with visual hallucination. *IEEE Robotics and Automation Letters*, 5(2):1672–1679, 2020.
- [21] Muhamad Risqi U Saputra, Chris Xiaoxuan Lu, Pedro Porto B de Gusmao, Bing Wang, Andrew Markham, and Niki Trigoni. Graph-based thermal-inertial slam with probabilistic neural networks. *IEEE Transactions on Robotics*, 2021.
- [22] Junhwa Hur and Stefan Roth. Optical flow estimation in the deep learning age. In *Modelling Human Motion*, pages 119–140. Springer, 2020.
- [23] Moritz Menze and Andreas Geiger. Object scene flow for autonomous vehicles. In *Proceedings of the IEEE conference on computer vision and pattern recognition*, pages 3061–3070, 2015.
- [24] Xun Huang and Serge Belongie. Arbitrary style transfer in real-time with adaptive instance normalization. In *Proceedings of the IEEE international conference on computer vision*, pages 1501–1510, 2017.
- [25] Xun Huang, Ming-Yu Liu, Serge Belongie, and Jan Kautz. Multimodal unsupervised image-to-image translation. In *Proceedings of the European conference on computer vision (ECCV)*, pages 172–189, 2018.
- [26] Ian Goodfellow, Jean Pouget-Abadie, Mehdi Mirza, Bing Xu, David Warde-Farley, Sherjil Ozair, Aaron Courville, and Yoshua Bengio. Generative adversarial networks. *Communications of the ACM*, 63(11):139–144, 2020.
- [27] Jun-Yan Zhu, Taesung Park, Phillip Isola, and Alexei A Efros. Unpaired image-to-image translation using cycle-consistent adversarial networks. In *Proceedings of the IEEE international conference on computer vision*, pages 2223–2232, 2017.
- [28] Ming-Yu Liu, Thomas Breuel, and Jan Kautz. Unsupervised image-to-image translation networks. *Advances in neural information processing systems*, 30, 2017.
- [29] Younggun Cho, Hyesu Jang, Ramavtar Malav, Gaurav Pandey, and Ayoung Kim. Underwater image dehazing via unpaired image-to-image translation. *International Journal of Control, Automation and Systems*, 18(3):605–614, 2020.
- [30] Li Xu, Jimmy Ren, Qiong Yan, Renjie Liao, and Jiaya Jia. Deep edge-aware filters. In *International Conference on Machine Learning*, pages 1669–1678. PMLR, 2015.
- [31] Yanmei Luo, Dong Nie, Bo Zhan, Zhiang Li, Xi Wu, Jiliu Zhou, Yan Wang, and Dinggang Shen. Edge-preserving mri image synthesis via adversarial network with iterative multi-scale fusion. *Neurocomputing*, 452:63–77, 2021.
- [32] Stephan R. Richter, Zeeshan Hayder, and Vladlen Koltun. Playing for benchmarks. In *IEEE International Conference*

- on *Computer Vision, ICCV 2017, Venice, Italy, October 22-29, 2017*, pages 2232–2241, 2017. doi: 10.1109/ICCV.2017.243. URL <https://doi.org/10.1109/ICCV.2017.243>.
- [33] Teledyne FLIR. Flir Thermal Sensing for ADAS. <https://www.flir.com/oem/adas>, 2022.
- [34] Seungsang Yun and Ayoung Kim. Sthereo: Stereo thermal dataset for research in odometry and mapping. In *Proceedings of the IEEE/RSJ International Conference on Intelligent Robots and Systems (IROS)*, 2022.
- [35] Zachary Teed and Jia Deng. Raft: Recurrent all-pairs field transforms for optical flow. In *European conference on computer vision*, pages 402–419. Springer, 2020.
- [36] Shihao Jiang, Dylan Campbell, Yao Lu, Hongdong Li, and Richard Hartley. Learning to estimate hidden motions with global motion aggregation. In *Proceedings of the IEEE/CVF International Conference on Computer Vision*, pages 9772–9781, 2021.
- [37] Haofei Xu, Jing Zhang, Jianfei Cai, Hamid Rezaatofighi, and Dacheng Tao. Gmflow: Learning optical flow via global matching. In *Proceedings of the IEEE/CVF Conference on Computer Vision and Pattern Recognition*, pages 8121–8130, 2022.
- [38] Javad Zolfaghari Bengar, Abel Gonzalez-Garcia, Gabriel Villalonga, Bogdan Raducanu, Hamed Habibi Aghdam, Mikhail Mozerov, Antonio M Lopez, and Joost van de Weijer. Temporal coherence for active learning in videos. In *2019 IEEE/CVF International Conference on Computer Vision Workshop (ICCVW)*, pages 914–923. IEEE, 2019.
- [39] Daniel J Butler, Jonas Wulff, Garrett B Stanley, and Michael J Black. A naturalistic open source movie for optical flow evaluation. In *European conference on computer vision*, pages 611–625. Springer, 2012.
- [40] Soonmin Hwang, Jaesik Park, Namil Kim, Yukyung Choi, and In So Kweon. Multispectral pedestrian detection: Benchmark dataset and baseline. In *Proceedings of the IEEE conference on computer vision and pattern recognition*, pages 1037–1045, 2015.
- [41] Matthew Johnson-Roberson, Charles Barto, Rounak Mehta, Sharath Nittur Sridhar, Karl Rosaen, and Ram Vasudevan. Driving in the matrix: Can virtual worlds replace human-generated annotations for real world tasks? In *2017 IEEE International Conference on Robotics and Automation (ICRA)*, pages 746–753. IEEE, 2017.
- [42] Haoyang Zhang, Ying Wang, Feras Dayoub, and Niko Sunderhauf. Varifocalnet: An iou-aware dense object detector. In *Proceedings of the IEEE/CVF Conference on Computer Vision and Pattern Recognition*, pages 8514–8523, 2021.